IOPscience iopscience.iop.org

Home Search Collections Journals About Contact us My IOPscience

Carbon p-electron induced magnetic ordering in Zn-implanted 6H–SiC: experimental observation and theoretical calculation

This content has been downloaded from IOPscience. Please scroll down to see the full text.

2016 Mater. Res. Express 3 056103

(http://iopscience.iop.org/2053-1591/3/5/056103)

View the table of contents for this issue, or go to the journal homepage for more

Download details:

IP Address: 218.22.21.14
This content was downloaded on 11/08/2016 at 02:42

Please note that terms and conditions apply.

IOP Publishing Mater. Res. Express 3 (2016) 056103 doi:10.1088/2053-1591/3/5/056103

Materials Research Express

RECEIVED
28 February 2016

REVISED
24 April 2016

ACCEPTED FOR PUBLICATION
30 April 2016

PUBLISHED
16 May 2016

PAPER

Carbon p-electron induced magnetic ordering in Zn-implanted 6H–SiC: experimental observation and theoretical calculation

Qiang Li[1,2,3,4], Juping Xu[3], Jiandang Liu[3] and Bangjiao Ye[3,4]

[1] Institute of High Energy Physics, Chinese Academy of Sciences (CAS), Beijing 100049, People's Republic of China
[2] Dongguan Neutron Science Center, Dongguan 523803, People's Republic of China
[3] State Key Laboratory of Particle Detection and Electronics, University of Science and Technology of China, Hefei, 230026, People's Republic of China
[4] Author to whom any correspondence should be addressed.

E-mail: qiangli@ihep.ac.cn (Qiang Li) and bjye@ustc.edu.cn (Bangjiao Ye)

Keywords: 6H-SiC crystal, ions implantation, defect-induced ferromagnetism, positron annihilation spectroscopy, first-principle calculations

Abstract

We observed clear ferromagnetic ordering in 6H–SiC crystal bombarded with zinc ions, and presented a detailed investigation of magnetic properties in this sample. The magnetization of Zn-implanted 6H–SiC fell and rose with annealing temperature from 500 °C to 1100 °C. Meanwhile, amount of oxygen penetrated lattices and combined with Si-bonds after 1100 °C annealing. Using *ab initio* calculations based on density functional theory, we confirm that Zn ions play a role in the origin of ferromagnetism, while the localized moment is mainly comes from C2p electrons surrounding the foreign particle (which is Zn in this work). Silicon vacancies can provide localized moment about 2.0 $\mu B/V_{Si}$ and form stable ferromagnetic interaction at room temperature. Oxygen may facilitate this coupling and no need of V_C-mediation any more. The calculations are consistent with experimental results. We concluded that the dangling C2p bonds are fundamental cause of magnetic ordering in whatever microstructures in 6H–SiC crystal. The type of foreign impurities is not crucial factor for the magnetic origin in such carbon-based materials.

1. Introduction

In the field of spintronics, many researches obtained significant progresses in the investigation of defect-induced ferromagnetism (DIM), which referred to as 'd0-magnetism' in contrast to traditional ferromagnetism containing partially filled d or f bands. However, many problems still remain to be resolved. DIMs challenge the basic understanding of ferromagnetic origin and provide potential for spintronic applications [1, 2]. Thus, they are continuously attracting research interest. Unexpected ferromagnetism was first discovered in carbon-based materials, and subsequently was observed from various oxides such as HfO_2, TiO_2, and ZnO [3–5]. The localized magnetic moments in these oxides were normally considered to be arising from s-p state spin polarization induced by cationic defects [6, 7].

SiC is a promising spintronic material due to its outstanding properties such as high breakdown field and thermal conductivity, large saturation drift velocity of carries, and chemical stability [8]. It is also considered as potential material for application in quantum information and diluted magnetic semiconductors in recent reports [9–12]. Thus, investigation of DIMs in SiC will have great significance on many fields. Few experiments on 'd0-magnetism' in SiC material have been reported thus far. Even though some progresses were acquired in research of magnetic origin, the experimental results are very different from that in oxide semiconductors. For non-magnetic doped SiC, the ferromagnetic coupling was normally attributed to the impurity related defect-complexes, such as Cu_{Si}–V_{Si} in Cu-implanted 6H–SiC, or Al_{Si}–V_{Si} in Al-doped 4H–SiC [13, 14]. Ferromagnetism was also observed in un-doped SiC powder or crystals [15, 16]. Chen *et al* demonstrated that the ferromagnetism in neutron-irradiated 6H–SiC arise from complex defects of V_C–V_{Si}, while Zhou *et al*

© 2016 IOP Publishing Ltd

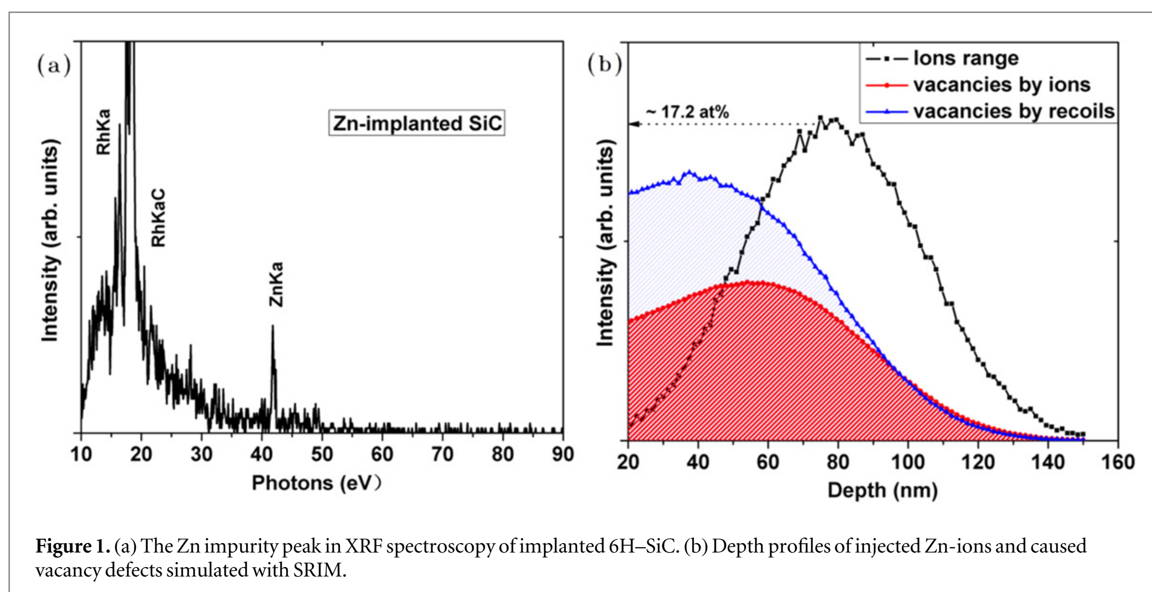

Figure 1. (a) The Zn impurity peak in XRF spectroscopy of implanted 6H–SiC. (b) Depth profiles of injected Zn-ions and caused vacancy defects simulated with SRIM.

observed an apparent drop of saturation magnetization with the formation of these divacancies in Ne-implanted 6H–SiC [17, 18]. Therefore, the dependence of ferromagnetism on the type of foreign impurities is under debate. Weather the particle is vital factor for magnetism in SiC material or not? Zhao *et al* predicted the silicon vacancies can induce localized moment about 2.0 $\mu B/V_{Si}$ in 3C–SiC and the nitrogen play a role in reducing the formation of vacancies [19]. Similar to Cu and Al, Zinc as nonmagnetic element has an advantage in excluding contribution from uncontrolled magnetic clusters. In this work, we present a detailed study of 6H–SiC implanted with Zn. The necessity of Zinc element for magnetic origin and the relationship between ferromagnetism and defects was systematically investigated by experiments and theoretical calculations. These results could promote further understanding of DIMs in carbon-based materials.

2. Experimental

6H–SiC single crystals (0.35 mm thickness) were obtained commercially from the Chinese Academy of Sciences (Shanghai). They were cut into a size of 6×8 mm^2 and then carefully decontaminated with ultrasonic acetone. Injection experiment was performed using ion implanter at the Beijing Normal University. Zn-ions at 160 keV were implanted into the polished surface of 6H–SiC crystals at room temperature to a fluence of 1×10^{17} cm^{-2}. The processes maintained a base pressure of 2.2×10^{-4} Pa and nearby controlled room temperature. X-ray fluorescence (XRF) spectroscopy only displayed Zn impurity peak after implantation, as shown in figure 1(a). This indicates the other elements like Fe, Co, Ni, etc in wafers was lower than detection limit of XRF. We did not detect the trace elements with other means, while the diamagnetic curves of raw wafers were confirmed closely. Average Zn-implanted profile together with vacancies simulated by Stopping and Ranges of Ions in Matter (SRIM) program is shown in figure 1(b).

The irradiated layer was approximately 120 nm range (20–140 nm) and the implanted peak of atomic concentrations is about 17.2 at% at 80 nm. The red and blue regions represent the content of vacancy defects caused by implanted ions and recoils. The track directions of Zn-ions were strongly changed by target lattice scattering, causing vacancy-related defects during recoiling stronger than that of implantation. The vacancies distribute from surface into implanted region, and the profile is different from that of Zn-ions. After implantation, sample was isochronally annealed at different temperatures (from 500 °C to 1100 °C) for 5 min in air. Before and after each annealing step, room-temperature magnetic properties were measured by vibrating sample magnetometer. For comparison, a carbon-irradiated 6H–SiC crystal was also prepared under the identical conditions with carbon energy of 80 keV and to a fluence of 2×10^{17} cm^{-2}. The sample structures and implanted-ions states were characterized by Raman spectroscopy and x-ray photoelectron spectroscopy (XPS), respectively. Positron annihilation technique was used to investigate the defective condition in samples. First-principles calculations based on density functional theory (DFT) were also employed to verify the experimental results and to provide further insight in the origin of ferromagnetism in 6H–SiC crystals.

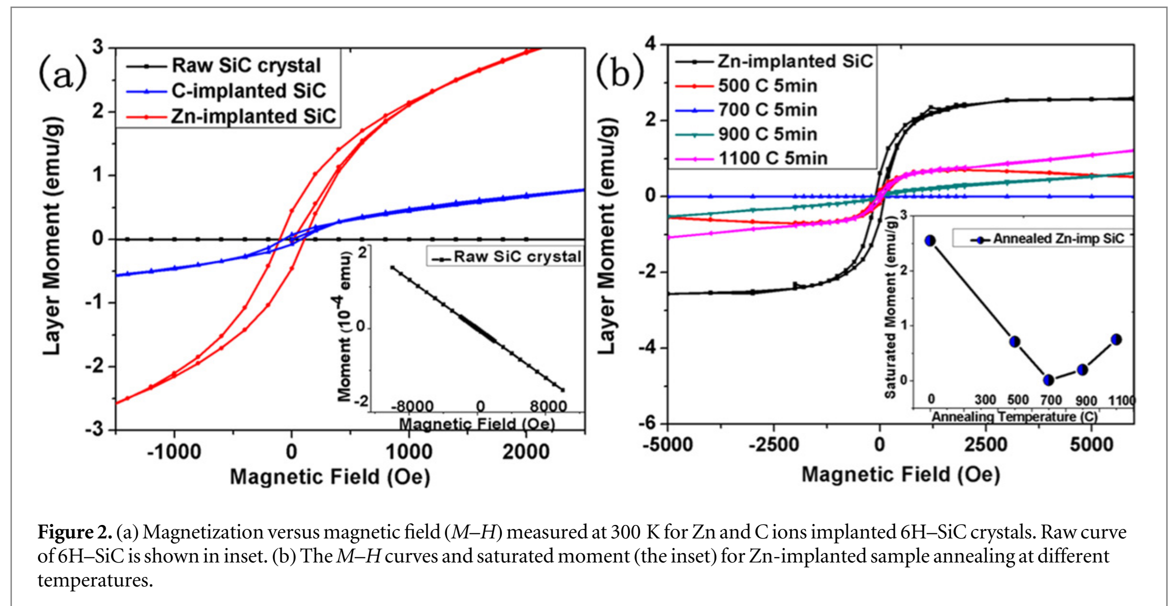

Figure 2. (a) Magnetization versus magnetic field (*M–H*) measured at 300 K for Zn and C ions implanted 6H–SiC crystals. Raw curve of 6H–SiC is shown in inset. (b) The *M–H* curves and saturated moment (the inset) for Zn-implanted sample annealing at different temperatures.

3. Results and discussion

The magnetic properties of Zn and C-implanted 6H–SiC crystals are displayed in figure 2. The raw 6H–SiC wafer resulted in a diamagnetic behavior (see inset of figure 2(a)), indicating that the samples did not contain any magnetic impurities or impurities were insignificant. The diamagnetic background influences was subtracted from the magnetic curves. Room temperature ferromagnetism could be observed in implanted samples, and the magnetizations were treated to mass normalization for injected layers.

As shown in figure 2(a), the C-implanted 6H–SiC displays obvious hysteresis with coercivity field (H_C) of approximately 75 Oe. The saturation magnetization (M_S) is about 0.24 emu g^{-1} with magnetic field increasing to 300 Oe. C-implantation does not introduce any impurities into SiC. The well-defined hysteresis indicates that the ferromagnetism is attributed to induced defects. This result is consistent with previous reports of neutron or Ne-implantation experiments [18, 20]. The M_S in Zn-implanted sample is about 2.0 emu g^{-1} at 1000 Oe, which is eight times larger than that of C-implanted sample. The H_C was approximately 160 Oe. As analyzed in SRIM simulation, the inject-induced defects should be considered to influence the magnetic property in this sample. However, comparing with C-implanted sample, there is a remarkable change in both the M_S and H_C for Zn-implanted sample, even though the fluence is only half of C ions. Defects alone are unlikely to be the only factor that influences the magnetic property in Zn-implanted 6H–SiC. It seems that the Zn as well as other particles (like Cu or Al) may also play a significant role in magnetic origin in SiC crystals. Paramagnetic component after magnetic field greater than 1000 Oe might be attributed to isolated moments of ions, which are located in low concentrated regions as shown in figure 1. The magnetic behaviors of isochronal annealed Zn-implanted sample are shown in figure 2(b). The paramagnetic components were subtracted from the curves. Unexpectedly, the ferromagnetic component first reduces and then increases with annealing process. As shown in the inset, a reduction of almost 70% of the magnetization was observed after the sample annealed at 500 °C. The sample annealed at 700 °C shows a further reduction of the magnetization. Almost linear response of *M–H* curve is observed, which indicates a paramagnetic behavior. Noteworthy, very different results were obtained after annealing at temperatures greater than 700 °C. A weak increase of magnetization appears after the sample annealed at 900 °C. Furthermore, an obvious increase was observed after 1100 °C annealing. Well-defined ferromagnetic loop was retrieved. Lattice recovery or ions migration usually occurs after sample annealing in higher temperature. This annealing behavior of magnetization further indicates that the ferromagnetism in Zn-implanted sample may arise from different sources. We employed Raman spectroscopy and positron annihilation technique to investigate micro-structural changes during annealing and the results are shown in figure 3.

The Raman spectra were measured using a 514.5 nm excitation line from an Ar^+ ion laser. The folded transverse optic (FTO) mode of SiC was observed at 151.1 cm^{-1}, indicating that the samples were 6H polymorphs [21]. The expected modes locate at 766 cm^{-1} = $FTO^{6/6}$, 789 cm^{-1} = $FTO^{2/6}$, and 965 cm^{-1} = FLO were also observed [22]. Raw sample shows sharp peak of FTO mode, indicating a good crystallinity of 6H–SiC. Induced defects undermined the lattice vibrational structure, leading to the peaks disappearing after implantation. As the annealing temperature increase, the peaks are retrieved and

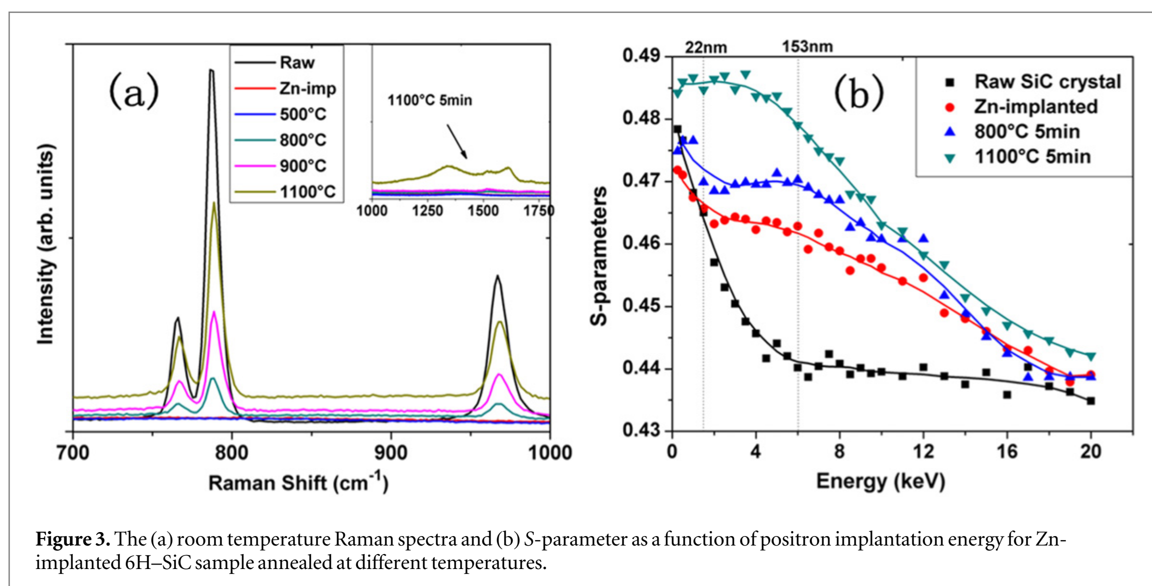

Figure 3. The (a) room temperature Raman spectra and (b) S-parameter as a function of positron implantation energy for Zn-implanted 6H–SiC sample annealed at different temperatures.

subsequently became longer, which is due to the recovery of ordered lattice vibrations. After sample annealing at 1100 °C, broadening peak envelopes appear at range of 1300–1700 cm^{-1}, as shown in the inset. These vibration modes are more likely related to the enrichment state of carbons instead of characteristic peaks of 6H–SiC.

The generation and annealing behavior of defects were detected by positron annihilation spectroscopy, which was proved to be an effective tool for detecting the vacancy-defects in materials [23]. Due to strong Coulomb repulsion from the positive ion cores, positrons have a high affinity to be captured by vacancy defects. Because of the reduced electron density and annihilation rate of those positrons with high-momentum core electrons at vacancy site, the Doppler broadening of 511 keV annihilation peak will become narrower than that of bulk annihilation. The Doppler broadening of annihilation peak was characterized by S-parameters, which defined as a fraction of counts in central area of this peak [24]. Thus, positrons trapped in vacancy defects will result in an increase in S-parameters. As shown in figure 3(b), compared with the raw sample, significant increase of S-parameters was observed in Zn-implanted SiC crystal. The sample surface usually exhibit high S-parameters due to the formation of positronium atoms [25]. V_{Si}-related vacancies as dominant positron trapping defects are heavily caused in implanted layer, and are considered to be responsible for S-parameters increase. The thickness of defect layer reflected in S–E curve is about 130 nm, which cover the whole injected region simulated by SRIM. The S_d-parameter in injected layer is about 0.465, and S_b-parameter in substrate layer is about 0.44, then $S_d/S_b \approx 1.057$–1.05. From a previous point of view, the defects are mainly mono- or divacancies [26]. Unexpectedly, annealing changes of these defects deviated from the demonstrated results in Raman spectra. The S-parameters increase after annealing at 800 °C and then show further rapid increase at an annealing temperature of 1100 °C, indicating that more vacancies were merged during annealing process. For the curve after 1100 °C annealing, the S_d-parameters is about 0.485, and then $S_d/S_b \approx 1.102 > 1.05$. These results show that a substantial increase of V_{Si} might be caused by defects agglomeration. Some V_{Si} are merged into larger cavity formation. On the other hand, electron paramagnetic resonance spectra reveal that implantation-induced carbon vacancies are reduced after annealing at 800 °C and disappeared after annealing at higher temperature.

The changes of Raman spectra and S–E curves after annealing reflect that recovery of inject-induced lattice damages, generation and agglomeration of V_{Si}-related defects may be simultaneous during annealing process. However, the cause of V_{Si} increase is not clearly explained in above experiments. XPS spectra detected lot of oxygen in 1100 °C annealed sample, which had been etched by Ar ions for 90 s to remove surface adsorption and expose Zn-ions for analysis. The result is shown in figure 4(a). In this result, It is clear that 6H–SiC was oxidized after annealing temperature at 1100 °C, and penetrated oxygen may bonded with lattice atoms [27].

The binding energy of Zn2p3/2 is located at 1022.0 eV and the energy gap between Zn2p3/2 and 2p1/2 is 23.1 eV, as shown in figure 4(b). After annealing at 1100 °C, the two peaks shift to the left (to 1021.1 eV and 1044 eV, respectively). Since Zn does not show negative valence and the binding energy of Zn^0 is normally less than that of Zn^{2+}, the Zn-ions in as-implanted sample are not zero valence [28]. Decrease of binding energy might be due to the deoxidization of Zn-ions [29]. Previous report pointed the difficulty of distinguishing Zn^{2+} and Zn^0 states experimentally using Zn2p peak, while auger spectra peaks can do this (the auger peaks of Zn^{2+} and Zn^0 are located ~986 eV and ~992 eV, respectively) [30]. As shown in inset, an apophysis was observed at ~992 eV, while no any hint of auger peak was observed at nearby ~986 eV (marked by arrow). Therefore, the left

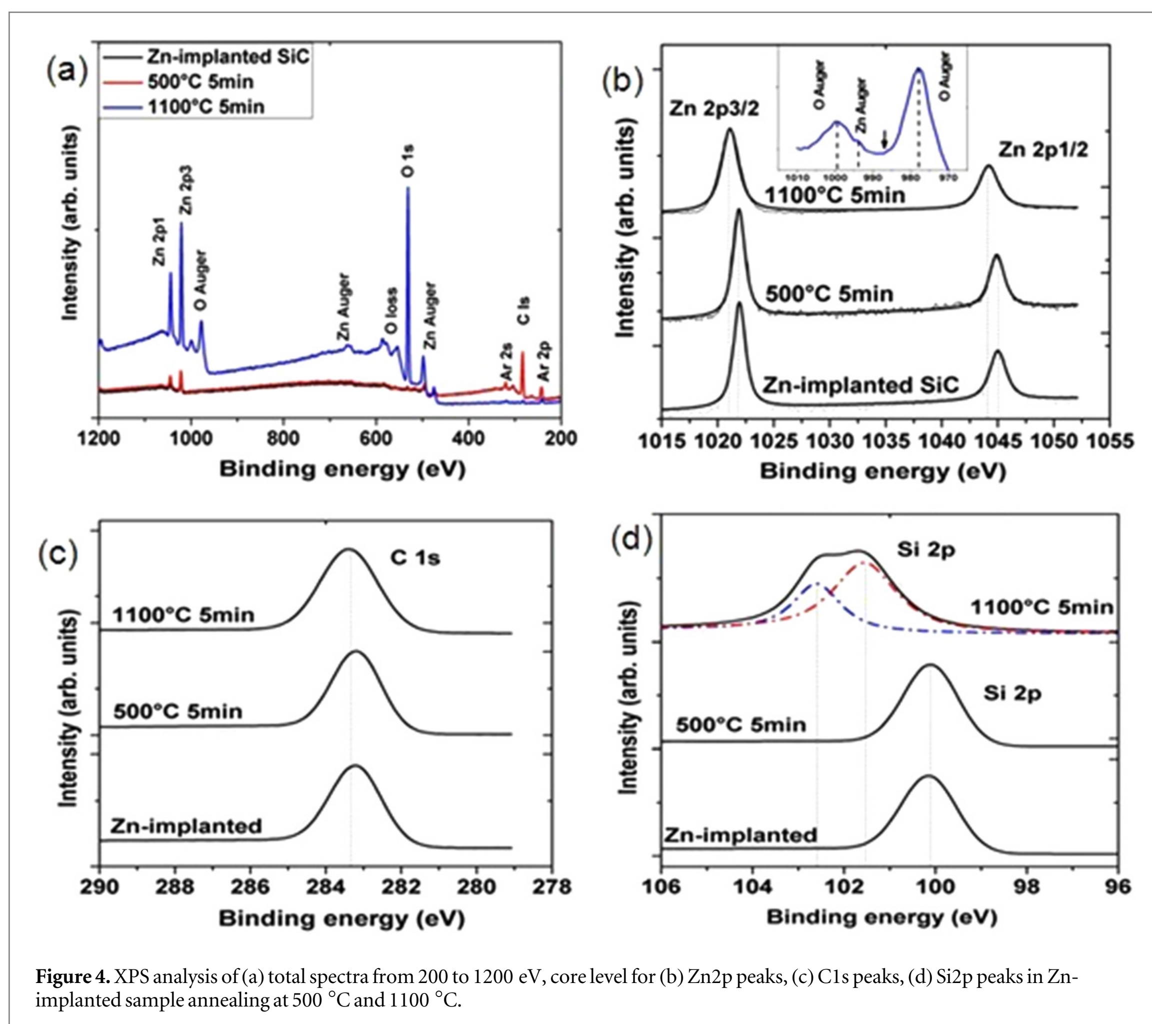

Figure 4. XPS analysis of (a) total spectra from 200 to 1200 eV, core level for (b) Zn2p peaks, (c) C1s peaks, (d) Si2p peaks in Zn-implanted sample annealing at 500 °C and 1100 °C.

movement of Zn2p peaks probably due to Zn-ions from the substitutional Si positions into interstitial lattice and form metal clusters, instead of combining with oxygen to form Zn–O bond. The C1s peak in raw sample locates at 282.6 eV, corresponding to C–Si bond in 6H–SiC crystal [31]. Figure 4(c) shows the binding energy increase to 283.2 eV after Zn-implantation, indicates a weakened anionic states of carbon in implanted layer [32]. This may be related to dangling bonds of carbons caused by induced-defects. The binding energy slightly increases with the annealing temperature. Meanwhile, the Si2p peak also shift to the left (increase) from 100.2 eV to an asymmetric peak after annealing at 1100 °C, as shown in figure 4(d). This peak can be fitted by two Gaussian curves. The high binding energy peak (blue dashes) located at 102.6 eV is related to the Si–O bonds. SiC heating in 1100 °C will reacts with oxygen to form SiO_2, and the weight of sample increase [27]. Zn is more easily oxidized than Si, while no hints of Zn–O bonds were detected. This may be because Zn mainly distributed in a thin implanted-layer in the depth about 100 nm in SiC crystal. During annealing, oxygen more likely to be contact with Si, while Zn tend to form metal clusters in their high concentration region.

Following the increase of annealing temperature, Zn-implantation induced damages were repaired continuously. Meanwhile, sample was oxidized after heating in higher temperature. Penetrated oxygen combined with Si-atoms to form Si–O bonds, and leave lots of V_{Si}-related clusters in the crystal, which result in significant increase of *S*-parameters in *S*–*E* curves. On the other hand, Zn-ions from the substitutional Si positions into interstitial lattices may also lead to increase of Si-vacancies. The room temperature ferromagnetism in Zn-implanted sample typically arises from different sources. And their annealing changes of magnetization can divided into two stages. Firstly, the magnetization declined with the temperature increase. In this stage the ferromagnetism probably relevant to Zn-ions or Zn-related defects. In the following stage the ferromagnetism should arise from V_{Si}-related defects. The magnetization increase may attributed to oxidization induce V_{Si} increase after higher temperature annealing. After annealing at 1100 °C, the ferromagnetism did not retrieved to the initial value of as-implantation. This may be because part of magnetic moments from Zn-ions had been irreversibly weakened, since the Zn-clusters were formed during annealing process.

It seems that Zn ions as well as other nonmagnetic atoms like Cu and Al could introduce ferromagnetism in SiC crystal. In order to have a completely physical picture on the work, a series of first-principle calculations

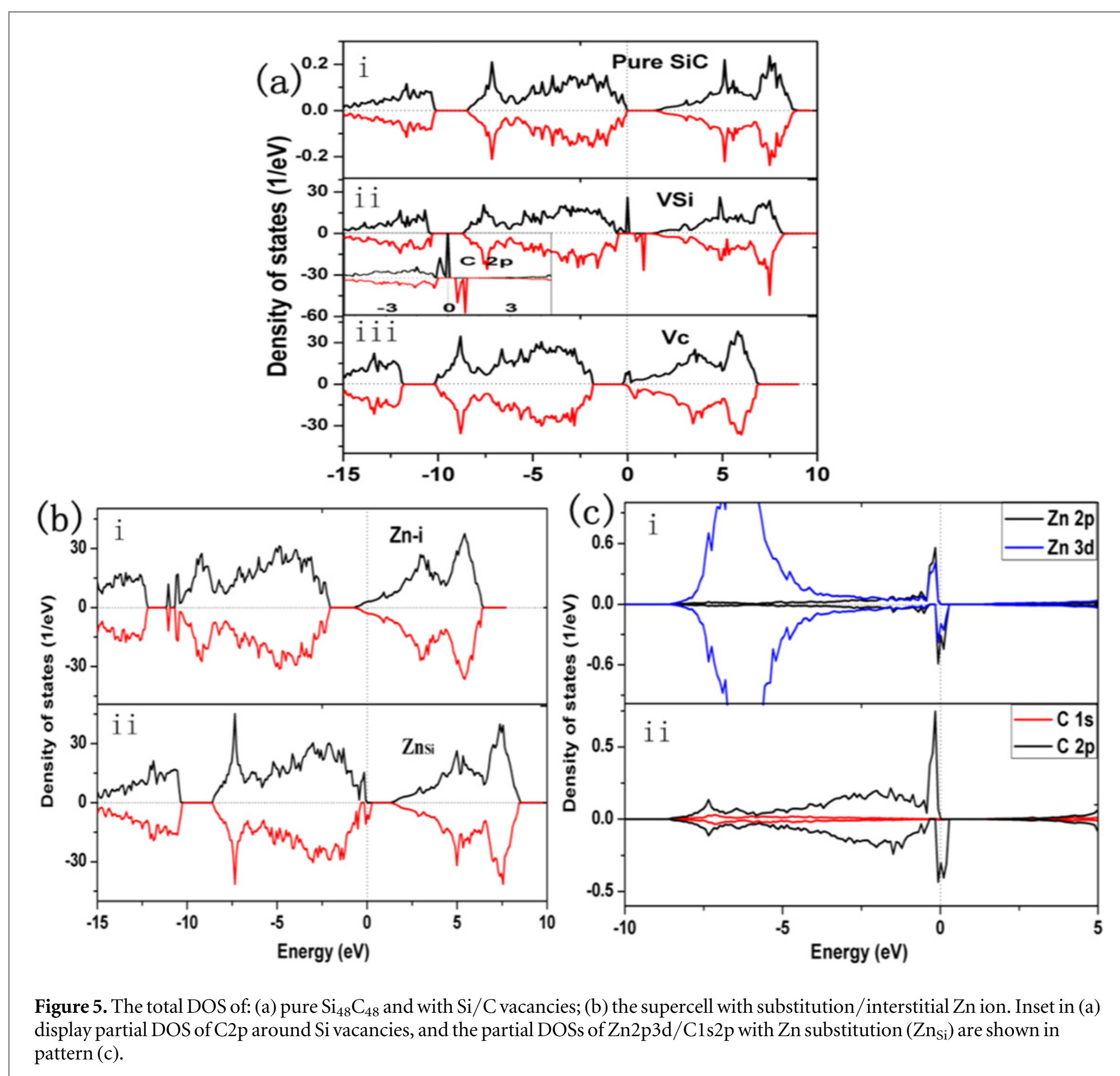

Figure 5. The total DOS of: (a) pure $Si_{48}C_{48}$ and with Si/C vacancies; (b) the supercell with substitution/interstitial Zn ion. Inset in (a) display partial DOS of C2p around Si vacancies, and the partial DOSs of Zn2p3d/C1s2p with Zn substitution (Zn_{Si}) are shown in pattern (c).

based on DFT were performed using the Vienna *ab initio* simulation package [33]. The Perdew–Burke–Ernzerh potentials were employed, and the general gradient approximation was used to describe the exchange correlation energy functional. We built $3 \times 2 \times 2$ SiC super-cell with 6H-structure, which contains 48 C-atoms and 48 Si-atoms for the calculation. The cases of one C/Si vacancy and/or Zn impurity at center of super-cell were firstly taken into account for discussion. For the Brillouin-zone sampling, $4 \times 4 \times 4$ Monkhorst-Pack k-mesh was used for the structural optimization and static computation process. The plane wave cut off energy was set to 400 eV, and the relaxed Hellman–Feynman force on each ion was less than 0.01 eV Å^{-1} during the optimization. Since the defect concentration is 2.1% for supercell contain one vacancy or Zn-atom, we only relaxed atoms around the defect point during the optimization (ISIF = 2). Figure 5 shows the results of density of electronic states (DOS) for pure and defected 6H–SiC supercell systems.

Perfect $Si_{48}C_{48}$ supercell in figure 5(a)–(i) display no spin polarization emerging around the Fermi energy level which is near the top of valence band, thus the material show nonmagnetic property. The valence electron shells of Si atom are $3s^2 3p^2$. In the structure with a Si taken away, the dangling bonds of C2p electrons are introduced around the vacancy, and obvious spin-split impurity bands are generated near the top of valence band, as shown in figure 5(a)–(ii). The total magnetic moment value of whole supercell is about 2.0 μB/V_{Si}. We calculated the atomic moment of V_{Si} within the Wigner–Seitz radius, the value is about 1.0 μB (which is related to the radius during static process). The results indicate that the localized moment arise from carbon dangling bonds around the V_{Si} (0.26 μB/electron). Differently, the impurity bands caused by carbon vacancy are mainly located at bottom of conduction band. The Fermi level was shifted to the bottom of conduction band. Although the total moment of $Si_{48}C_{47}V_C$ is not zero, it is not localized around the carbon vacancy. The atomic moment of V_C is only 0.65 μB (less than 40% of total moment), which is widely distributed in the nearby silicon and carbon sites. Since the electronegativity of carbon is higher than that of silicon, the unpaired electrons around carbons atoms should be more localized than those around silicon atoms [34]. On the other hand, in relaxation process

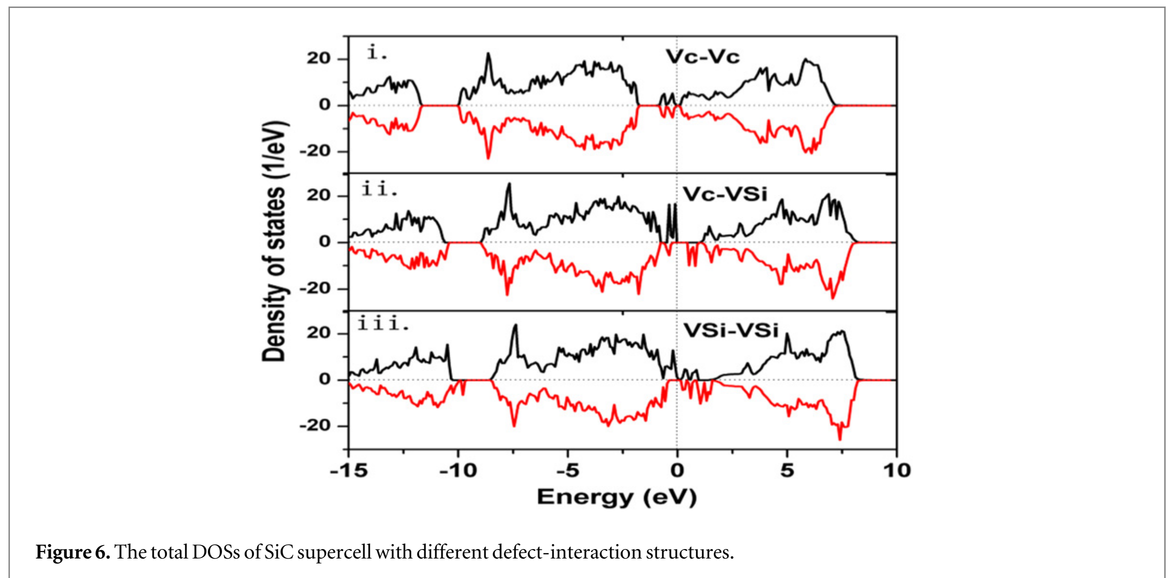

Figure 6. The total DOSs of SiC supercell with different defect-interaction structures.

the V_C will display important '*J–T* distortion', which will lead to the disappearance of spin polarization, while this phenomenon would not occur in V_{Si} structures [35]. Magnetic coupling is relevant to the degree of localized magnetic moments. Thus, carbon vacancy is hardly introducing obvious ferromagnetism in the SiC system, which is in good agreement with our experimental discussions.

The Zn atom in SiC supercell has two situations: Zn located at interstitial site of octahedral which consist of four carbon and four silicon atoms; or the Zn substitute of a Si and nearby four carbon atoms. As shown in the figure 5(b), interstitial Zn may result in slight expansion of surrounding lattices, while does not introduce unpaired electrons in the supercell. The Zn3d bands are below the Fermi level about 8 eV, and display symmetrical spin structure. The total magnetic moment of this structure is nearly zero. Differently, the substitutional Zn2p3d electrons introduced polarized impurity bands near the Fermi level, which is across the top of valence band. The calculated localized atomic moment of this supercell is 1.18 μB (maintaining the Wigner–Seitz radius), which unexpectedly include the contributions of C2p electrons around Zn atoms, as shown in figure 5(c). For partial DOSs analysis, we found that the magnetic moment from polarized Zn2p3d electrons is 0.158 μB, which only 13% of the total localized moment. While the average contribution from around four carbon atoms is about 0.151 μB/C. These results indicate that the magnetism of SiC sample is mainly from spin-polarized carbon 2p electrons around interstitial Zn, not from Zn atoms themselves. In further speculation, the dangling C2p electrons maybe mainly source of magnetic ordering in nonmagnetic doping 6H–SiC crystals, meanwhile the type of foreign impurities (such as Cu, Al, He *et al*) are not crucial factor for magnetic origin in such carbon-based materials. This analysis corroborates the results and discussions of our experiments.

We discussed magnetic coupling between the vacancy defects. There are three cases of magnetic interaction between silicon/carbon vacancies, as shown in figure 6. We only discuss the nearest-neighbor structures, in which the distance of V_C–V_C (V_{Si}–V_{Si}) is 0.309 nm, and the V_C–V_{Si} spacing is 0.189 nm.

During full-relaxation process, the supercell with V_C–V_C structure arise defect-distortion as described in previous report. The spin polarizations of peripheral electrons disappear and the total moment of this supercell turns into zero. This confirms that the non-localized moments of carbon vacancies can not achieve stable magnetic coupling and introduce ferromagnetism in SiC material. In previous studies, the V_{Si}–V_C structure was considered mainly source of ferromagnetism in SiC. We introduced this structure and calculated the total moment of supercell and found to be still about 2.0 μB. The average magnetic moment from remained three carbon atoms is about 0.264 μB/C and the second-adjacent carbons show a small value (about 0.02 μB/C). The presence of V_C has not affected the value and localization degree of the magnetic moment of V_{Si}. Different from the He or Al in V_{Si}-related defects, the role of V_C may only be able to reduce formation of silicon vacancies so that they can be stably present in materials. We constructed the nearest-neighbor V_{Si}–V_{Si} structure and calculated magnetic coupling between them. The carbon between silicon vacancies attributes two parallel spin-polarized 2p electrons, and they are involved in ferromagnetic interaction with neighbor four C2p electrons. The schematic diagram of this magnetic coupling is shown in figure 7. From the perspective of simple magnetism, the results indicate that dangling C2p electrons from V_{Si}-related defects can provide localized moment and form stable ferromagnetic interaction without any induced impurity or carbon vacancy. Furthermore, we confirmed

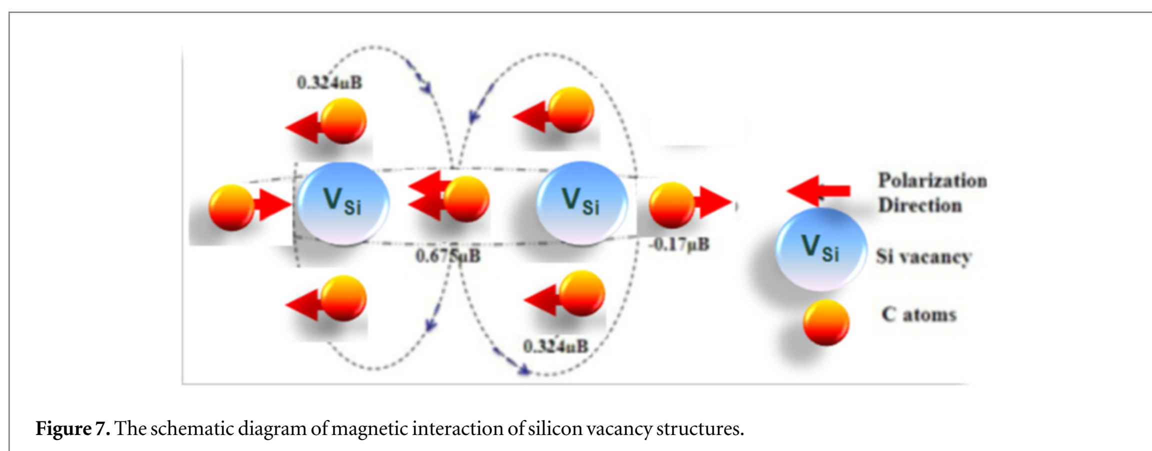

Figure 7. The schematic diagram of magnetic interaction of silicon vacancy structures.

that the carbon vacancies in SiC material are not involved in magnetic performance. This is in line with experimental findings.

4. Conclusion

In this work we investigated the magnetic properties of Zinc-irradiated 6H–SiC by both experimental and theoretical calculations. The results give strong evidence that the unpaired C2p electrons nearest-neighbor structure defects are radically responsible for the observed ferromagnetism. In this sample, the ferromagnetic performance is mainly arising from substitutional zincs and silicon vacancy-related defects. The zincs were proved not crucial factor for ferromagnetic origin in sample and carbon vacancies are not involved in magnetic coupling of silicon vacancies. Interestingly, it has been demonstrated that the localized moments of V_{Si} will disappear when replacing around carbons with silicones, while V_C may exhibit magnetism within graphite material. This provides valuable speculation that unpaired C2p-induced ferromagnetism maybe universal in SiC, graphitic and other carbon-based materials. Our studies give more insight into comprehending the phenomena of carbon-based materials and encouraging their future applications in spintronics.

Acknowledgments

This work is supported by the National Natural Science Foundation of China (Grant No. 11475165).

References

[1] Rainey K, Chess J, Eixenberger J, Tenne D A, Hanna C B and Punnoose A 2014 Defect induced ferromagnetism in undoped ZnO nanoparticles *J. Appl. Phys.* **115** 17D727
[2] Wang D D, Qi N, Jiang M and Chen Z Q 2013 Defects versus grain size effects on the ferromagnetism of ZrO_2 nanocrystals clarified by positron annihilation *Appl. Phys. Lett.* **102** 042407
[3] Esquinazi P, Spemann D, Hohne R, Setzer A, Han K H and Butz T 2003 Induced magnetic ordering by proton irradiation in graphite *Phys. Rev. Lett.* **91** 227201
[4] Venkatesan M, Fitzgerald C and Coey J 2004 Anisotropic ferromagnetism in substituted zinc oxide *Nature* **430** 630
[5] Sundaresan A, Bhargavi R, Rangarajan N, Siddesh U and Rao C N R 2006 Ferromagnetism as a universal feature of nanoparticles of the otherwise nonmagnetic oxides *Phys. Rev.* B **74** 161306R
[6] Peng H W, Xiang H J, Wei S H, Li S S, Xia J B and Li J B 2009 Origin and enhancement of hole-induced ferromagnetism in first-row d0 semiconductors *Phys. Rev. Lett.* **102** 017205
[7] Chanier T, Opahle I, Sargolzaei M, Hayn R and Lannoo M 2008 Magnetic state around cation vacancies in II–VI semiconductors *Phys. Rev. Lett.* **100** 026405
[8] Song B *et al* 2008 New experimental evidence for origin of ferromagnetism ordering in Fe-doped SiC *Physica* B **403** 2897–901
[9] Koehl W F, Buckley B B, Heremans F J, Calusine G and Awschalom D D 2011 Room temperature coherent control of defect spin qubits in silicon carbide *Nature* **479** 84–7
[10] Castelletto S *et al* 2014 A silicon carbide room-temperature single-photon source *Nat. Mater.* **13** 151–6
[11] Zheng H, Zhang Y, Yan Y, Lv Z, Yang H, Liu X, Gu Y and Zhang W 2014 Experimental observation and theoretical calculation of magnetic properties in Fe-doped cubic SiC nanowires *Carbon* **78** 288–97
[12] Lv Z C, Ma X P, Zheng H W, An R, Peng C X, Liu J D, Ye B J, Diao C L, Liu X Y and Zhang W F 2013 Room temperature ferromagnetism induced by N-ion implantation in 6H–SiC single crystal *Mater. Lett.* **93** 374–6
[13] Zheng H W *et al* 2013 Room-temperature ferromagnetism in Cu-implanted 6H–SiC single crystal *Appl. Phys. Lett.* **102** 142409
[14] Yu L *et al* 2010 Investigation of ferromagnetism in Al-doped 4H–SiC by density functional theory *Chem. Phys. Lett.* **496** 276
[15] Juliana M M and Gul R 2013 . Role of vacancies in the magnetic and electronic properties of SiC nanoribbons: an ab initio study *Phys. Rev.* B **87** 115428

[16] Zhou R-W, Liu X-C, Zhuo S-Y, Chen H-M, Shi B and Shi E-W 2015 Divacancies induced ferromagnetism in 3C-SiC thin films *J. Magn. Magn. Mater.* **374** 559–63
[17] Li L *et al* 2011 Rise and fall of defect induced ferromagnetism in SiC single crystals *Appl. Phys. Lett.* **98** 222508
[18] Liu Y *et al* 2011 Defect-induced magnetism in neutron irradiated 6H–SiC single crystals *Phys. Rev. Lett.* **106** 087205
[19] Zhao M, Pan F and Mei L 2010 Ferromagnetic ordering of silicon vacancies in N-doped silicon carbide *Appl. Phys. Lett.* **96** 012508
[20] Wang Y *et al* 2014 Disentangling defect-induced ferromagnetism in SiC *Phys. Rev.* B **89** 014417
[21] Lin S, Chen Z, Liang P, Jiang D and Xie H 2010 Room-temperature ferromagnetism of vanadium-doped 6H–SiC *Chem. Phys. Lett.* **496** 56–8
[22] Shi-Yi Z *et al* 2012 Defects mediated ferromagnetism in a V-doped 6H–SiC single crystal *Chin. Phys.* B **21** 067503
[23] Krause-Rehberg R and Leipner H S 1999 *Positron Annihilation in Semiconductors, Defect Studies* (*Springer Series in Solid-State Sciences* vol 127) (Berlin: Springer)
[24] Toivonen J, Hakkarainen T, Sopanen M, Lipsanen H, Oila J and Saarinen K 2003 Observation of defect complexes containing Ga vacancies in GaAsN *Appl. Phys. Lett.* **82** 1
[25] Zhang B Y *et al* 2011 Evidence of cation vacancy induced room temperature ferromagnetism in Li–N codoped ZnO thin films *Appl. Phys. Lett.* **99** 182503
[26] Droghetti A and Sanvito S 2009 Electron doping and magnetic moment formation in N-and C-doped MgO *Appl. Phys. Lett.* **94** 252505
[27] Jianlei K and Cao W 2014 Oxidation behavior of SiC whiskers at 600 °C–1400 °C in air *J. Am. Ceram. Soc.* **97** 2698–701
[28] Biesinger M C, Lau L W M, Gerson A R and Smart R C St 2010 Resolving surface chemical states in XPS analysis of first row transition metals, oxides and hydroxides: Sc, Ti, V, Cu and Zn *Appl. Surf. Sci.* **257** 887–98
[29] Wang C C *et al* 2012 Role of cobalt in room-temperature ferromagnetic Co-doped ZnO thin films *AIP Adv.* **2** 012182
[30] Feliu S Jr and Barranco V 2003 XPS study of the surface chemistry of conventional hot-dip galvanised pure Zn, galvanneal and Zn–Al alloy coatings on steel *Acta Mater.* **51** 5413–24
[31] Hornetz B, Michel H J and Halbritter J 1995 Oxidation and 6H–SiC–SiO_2 interfaces *J. Vac. Sci. Technol.* A **13** 767
[32] Akbar S, Hasanain S K, Abbas M, Ozcan S, Ali B and Ismat Shah S 2011 Defect induced ferromagnetism in carbon-doped ZnO thin films *Solid State Commun.* **151** 17–20
[33] Koch W, Holthausen M C and Chemist's A 2001 *Guide to Density Functional Theory* (Weinheim: Wiley, VCH)
[34] Wang Y *et al* 2015 Carbon p electron ferromagnetism in silicon carbide *Sci. Rep.* **5** 8999
[35] Zywietz A, Furthmüller J and Bechstedt F 2000 Spin state of vacancies: from magnetic Jahn-Teller distortions to multiplets *Phys. Rev.* B **62** 6854